Gondwana Research 22 (2012) 127–139

Contents lists available at SciVerse ScienceDirect

Gondwana Research

journal homepage: www.elsevier.com/locate/gr

Spatial distribution of seismic layer, crustal thickness, and Vp/Vs ratio in the Permian Emeishan Mantle Plume region

Jing Wu *, Zhongjie Zhang

State Key Laboratory of Lithospheric Evolution, Institute of Geology and Geophysics, Chinese Academy of Sciences, Beijing 100029, China

ARTICLE INFO

Article history:
Received 22 July 2011
Received in revised form 14 October 2011
Accepted 17 October 2011
Available online 7 November 2011

Handling Editor: A. Aitken

Keywords:
Late Permian
Emeishan mantle plume
Lithosphere rheology structure
Seismic energy release
Lithosphere modification

ABSTRACT

Seismological studies of lithospheric structure and rheology can provide important information regarding the lithosphere's interaction with the mantle plume and its successive deformation characterization. The Emeishan Large Igneous Province (ELIP) in eastern Tibet was probably produced by a Late Permian Emeishan mantle plume and experienced tectonically driven modifications during Mesozoic–Cenozoic, such as the eastward subduction of the Indian Ocean plate and roughly north-southward tectonic escape or middle crustal flow. The crustal responses to the Emeishan mantle plume and its modification from successive tectonic activities are still unclear. Here, we present the lithosphere rheology structure derived from seismic activity and the spatial distribution of seismic energy release, which records the lithospheric deformation from the Late Permian mantle plume activity and the Mesozoic–Cenozoic modifications. In addition, we estimate the crustal thickness and the average crustal Vp/Vs ratio from wide-angle seismic profiling and receiver function imaging. Our results demonstrate that the seismogenic layer thins away from the proposed center of the Emeishan mantle plume. The layer is approximately 24 km in depth beneath the center of the Emeishan mantle plume and approximately 10 km in depth beneath the margin of the plume, with corresponding crustal thinning and spatial variations of the average crustal Vp/Vs ratio. Distinctive patterns among crustal thickness, seismogenic layer and the average crustal Vp/Vs ratio are observed both east and west of the Xiao Jiang Fault (XJF). These remarkable features are interpreted to result from the modification of the Late Permian mantle plume, probably by tectonic escape in the west of the XJF and by a north-southward middle crustal flow in the east of the XJF.

1. Introduction

The hypothesis of the mantle plume was proposed by geophysicist W. Jason Morgan in 1971 and has been evaluated by laboratory experiments (Whitehead and Luther, 1975), seismology (Zhao, 2004, 2007; Zhao, 2009), geochemistry (Roy et al., 2002; Xu et al., 2004, 2007; Ernst, 2006; Cheng and Kusky, 2007; Wang et al., 2009; Chen et al., 2011; Su et al., 2011; Yu et al., 2011) and dynamical modeling (Yuen et al., 1993). A mantle plume is an upwelling of abnormally hot rock within the Earth's mantle. As the tops/heads of mantle plumes can partially melt when they reach shallow depths and pressure is reduced, they are thought to be the cause of volcanic centers, known as hotspots, and are the probable cause of flood basalts, which have catastrophic effects once the magma spills out onto the crust.

In the last 20 years, increasingly more evidence for lower-mantle plumes has been found with seismic tomography studies (Goes et al., 1999; Li et al., 2000; Zhao, 2001; Rhodes and Davies, 2001; Romanowicz and Gung, 2002; Ritsema and Allen, 2003; Montelli et al., 2004, 2006; Lei and Zhao, 2006; Zhao, 2009). When the top of a mantle plume meets the base of the lithosphere, it is expected to flatten out against this barrier, uplift the lithosphere bottom and undergo widespread decompression melting to form large volumes of basalt magma. Thus, the activity of a mantle plume should be imprinted in the lithosphere structure. However, the crustal responses to the mantle plume and its modification from successive tectonic activities are still unclear. The Emeishan mantle plume (featured in the Emeishan Large Igneous Province — ELIP) is a unique place to study this phenomenon.

The ELIP is the only verified Large Igneous Province (LIP) in China. The Late Permian Emeishan continental flood basalts in southwestern China form a major part of the ELIP, which covers an area of 250,000 km^2 (Xu et al., 2001) from the eastern margin of the Tibetan Plateau to the western margin of the Yangtze block (Fig. 1). The Emeishan basalts in southwest China have attracted the attention of the scientific community in recent years because of their possible synchrony with the eruption of the Siberian traps and thus their possible relationship with the mass extinctions during the Late Permian (Chung and Jahn, 1995; Chung et al., 1998; Xu et al., 2001; Ali et al., 2002; Lo et al., 2002; Zhou et al., 2002; Courtillot and Renne, 2003; Wignall et al., 2009).

Chung and Jahn (1995) used the mantle plume model to explain the eruption of the Emeishan flood basalts in China. More research on a rigorous evaluation of the role of mantle plumes in the

* Corresponding author. Tel.: +86 10 82998229.
E-mail address: xianhua123@yahoo.com (J. Wu).

1342-937X/$ – see front matter
doi:10.1016/j.gr.2011.10.007

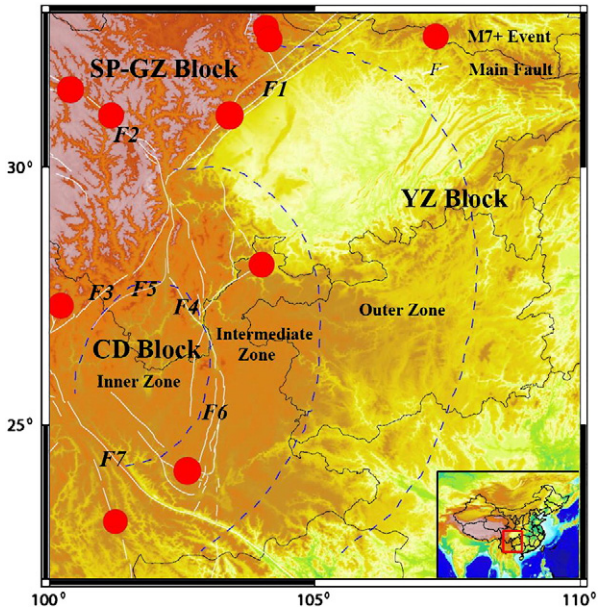

Fig. 1. ELIP distribution with geology, topography, earthquakes, and faults: *F1* Longmenshan Fault; *F2* Xianshui River Fault; *F3* Lijiang Fault; *F4* Zemuhe Fault; *F5* Jinhe Fault; *F6* Xiao Jiang Fault; *F7* Ailao Shan–Red River Fault. SP–GZ Block: Songpan–Ganzi Block; CD Block: Chuan Dian Block; YZ Block: Yangtze Block. Inner Zone, Intermediate Zone, and Outer Zone: the spatial distribution of the ELIP, separated by the blue curve. Inset: the red square is the location of the ELIP in China.

generation of this large igneous province has become available in the last 10 years (He et al., 2003; Xu et al., 2004; Zhang et al., 2006). A recent review of the Late Permian ELIP shows that 7 out of the 9 most convincing arguments in support of mantle plumes are found in the ELIP (Xu et al., 2007). In particular, sedimentology data show unequivocal evidence for a lithospheric doming event prior to the Emeishan volcanism. In addition, the presence of high-temperature magmas, the emplacement of an immense volume of magmas over a short time span, and spatial variation in the basalt geochemistry are all consistent with predictions of plume modeling. These observations strongly support the validity of the Late-Permian mantle plume hypothesis (Xu et al., 2007).

Seismic investigations can trace mantle plumes in modern, active hotspots, but are of limited benefit in identifying ancient plumes, mainly because geophysics provides us with a present snapshot of the structure of the Earth superposed on a long evolutionary history. The present structure of the Earth, as described by geophysics, can provide hints on whether the ancient plumes experienced any kind of tectonically driven modifications.

The Late-Permian mantle plume beneath ELIP experienced multiphased large-scale deformation from tectonic activities, such as the Indian oceanic plate eastward subduction (Wang and Gang, 2004; Lei et al., 2009) and/or tectonic escape (Molnar and Tapponnier, 1975; Yin and Harrison, 2000) or crustal flow (Clark and Royden, 2000; Zhang et al., 2009b; Bai et al., 2010a). These events would be expected to be recorded in elevated heat flow and the consequent attenuated brittle behavior of the lithosphere, i.e., the lower level of seismic energy release and the shallower focal depth of seismic events (Panza and Raykova, 2008; Zhang et al., submitted for publication). Tremendously deep geophysical experiments in last 30 years in the research area (mainly initiated with earthquake monitoring, Deng et al., 2011) have provided an excellent opportunity to understand the lithospheric response to mantle plume activity and its subsequent deformation. In this paper, we combine the lithospheric structure derived from deep seismic sounding (Cui et al., 1987; Xiong et al., 1993; Zhang et al., 2007; Deng et al., 2011) and receiver function imaging (Hu et al., 2003; Zhang et al., 2009a) with the distribution versus depth of earthquakes to assess the brittle properties of the highly sensitive Earth. A synoptic representation of the mechanical properties of the uppermost 60 km is provided, along with the seismicity, averaged over cells 1° by 1° in size. According to the rheology and structure of the lithosphere under southwest China, we investigate whether the lithosphere's structure with ancient plume activity was maintained under the ELIP. If the structure was maintained, it would mean that the lithosphere's structure was not superposed with prominent tectonically driven modification occurring since the formation of the ELIP, whereas if it was not maintained, then we need to determine what occurred with the ancient plume after the formation of the ELIP in the Late Permian. Our results show a systematic lateral variation of the seismic layer (brittle layer) from the inner to outer zones of the proposed Late Permian mantle plume (He et al., 2003; Xu et al., 2004). Our observed lateral/azimuthal variations of crustal thickness, the average crustal Vp/Vs ratio and the seismic layer thickness contradict the expected characteristics from a classic mantle plume. We attribute the discrepancy between the observed and the expected to the lithosphere enduring successive tectonic activities: the eastward Indian Ocean plate subduction and the nearly north-southward middle crustal flow or tectonic escape. The paper is structured as follows: first, a brief description of the tectonic setting is provided; then, the seismic rheology and lithosphere structure is presented; and finally, the lateral/azimuthal variations of crustal thickness, the average crustal Vp/Vs ratio, seismic layer thickness, and the corresponding tectonic implications are discussed.

2. Tectonic setting

The ELIP is located at the southwest of the Chinese continent. Fig. 1 shows the tectonic framework and spatial distribution of the topography and earthquake epicenters with magnitudes of $Ms \geq 7.0$ since 1970 in the ELIP region. The ELIP is displayed as three subzones (named the inner, intermediate and outer zones by Xu et al., 2004) that are circular or semi-circular in shape corresponding to the convergence belt of the three main sub-blocks, which are the SP–GZ (Songpan–Ganzi) block, the Yangtze block, and the CD (Chuan Dian) block. The Late Permian Emeishan basalts are erosional remnants of the voluminous mafic volcanic successions that occurred in the western margin of the Yangtze Craton, SW China. These successions are exposed in a rhombic area of 250 000 km^2 (Xu et al., 2001) bounded by the Longmenshan thrust fault in the northeast and the Ailao Shan Red River (ASRR) slip fault in the southwest (Fig. 1). The tectonic setting of the study area is highly complex, with the distribution of seven main faults concentrated in the west of the ELIP. The ELIP is one of the most active areas of earthquake activity in China, and nine strong earthquakes ($Ms \geq 7.0$) have occurred since 1970, including the disastrous Mw 7.9 Wenchuan Earthquake (May 12, 2008) on the Longmenshan Fault, which result in an enormous loss of life and property.

The Late Permian Emeishan mantle plume model is proposed initially from unambiguous evidence for a rapid crustal doming prior to the Emeishan flood volcanism (258–254 Ma) in southwest China (He et al., 2003). From the middle Permian–late Permian sedimentology and geochemistry of the volcanic successions (Xu et al., 2004), He et al. (2003) claimed a lithospheric uplift prior to the Emeishan volcanism, which was responsible for (1) the rapid sea-level fall recorded by a regression at the boundary between the middle Permian and upper Permian rocks in the western Yangtze craton and (2) the generation of clastic deposits surrounding the apex of the domal structure during the Permian. They divided the domal structure associated with the Emeishan Large igneous province into inner, intermediate and outer zones regarding the extent of erosion of the Maokou Formation. The boundary between the inner and the intermediate zones is the XJF (*F6* in Fig. 1) to the east, the Zemuhe Fault (*F4*) to the northeast, and the Jinhe Fault (*F5*) to the northwest. These faults controlled the rapid deposition of clastic deposits in canyons and on alluvial fans. The extent of erosion is most apparent (at

the impact site of the rising plume head, He et al., 2003) in the interior zone but is modest in the intermediate zone and generally minor in the outer zone. Spatial variation in the basalt geochemistry would result from the spatial zonation of mantle temperature, which would lead to systematic variations in the degree of melting (Campbell and Griffiths, 1990). In general, the domed region of the ELIP comprises thick (2000–5000 m) sequences of dominant low-Ti volcanic rocks and subordinate picrites (Chung and Jahn, 1995). The application of rare-earth element inversion techniques (McKenzie and O'Nions, 1991) reveals that the low-Ti lavas that originated at 60–140 km required 16% melting and a mantle temperature of >1500°. In contrast, the high-Ti lavas were generated at 75–100 km during events of much smaller degrees of melting (1.5%) and a lower mantle temperature (<1500°). The predominance of the thick low-Ti lavas in the inner zone suggests that the mantle beneath the core of the domal structure underwent a larger extent of partial melting than that under the marginal area. This suggestion combined with the occurrence of picrites in the inner zone is consistent with a hotter mantle beneath the dome center than beneath the dome periphery. A likely scenario is that a plume head was present underneath the inner zone.

However, some basalts and mafic complexes exposed in the Simao Basin, northern Vietnam (west of the ASRR Fault, *F7*), and in the Qiangtang terrain, the Lijiang–Yanyuan Belt and the Songpan active fold belt (northwest of the Longmenshan Fault, *F1*) make possible an extension of the ELIP (Chung et al., 1998; Xiao et al., 2003; Hanski et al., 2004). Some Emeishan-type basalts traced in southwest Yunnan and northern Vietnam may be related to the mid-Tertiary continental extrusion of Indochina relative to South China along the ASRR Fault (Tapponnier et al., 1990; Chung et al., 1997). The geological and geochemical evidence may suggest a successive deformation from a nearly southward tectonic escape/crustal flow around the eastern axis of the Tibetan plateau or the eastward subduction of Indian Ocean plate.

3. Seismic rheology and lithosphere structure

Most data on the ELIP are from geochemistry (Xu et al., 2007) and limited geophysical datasets. However, geophysics can provide important information about the velocity, temperature, electricity, and anisotropy of the deep Earth. To determine the present rheology and lithospheric structure of the ELIP, we offer three kinds of geophysical research for evaluating the ELIP: seismicity from events recorded by permanent stations; lithospheric structure from deep seismic sounding; and crustal composition from receiver function imaging in the studied area.

3.1. Lithosphere rheology structure: Seismic energy release pattern

The presence of a plume beneath the ELIP would be expected to be recorded in an elevated heat flow and the consequent attenuated brittle behavior of the lithosphere, i.e., the lower level of seismic energy release and shallower focal depths of seismic events (Panza and Raykova, 2008). To construct lithosphere rheology structure, we separate the ELIP, covering the area 100°–110°E, 22°–32°N, into 100 1° by 1° cells.

All the seismic events reported during the thirty-year period from 1980 to 2010 in the catalog of the China Earthquake Network Center (CENC) were characterized by considering a total of 100 contiguous cells. We compiled 8 profiles (profiles 1–8) in the area at different directions and shapes considering the spatial distribution of the ELIP (Fig. 2). The national seismic network commonly uses the Geiger method (Geiger, 1912) to locate the events while the hypo2000 (Klein, 2002) and hypoDD (Waldhauser and Ellsworth, 2000) codes are used by the regional seismic networks. The precision of the location of seismic events is commonly scaled either as level A (having an uncertainty of focal depth of $\delta d \leq 5$ km), B ($5 < \delta d \leq 15$ km), C ($15 < \delta d \leq 30$ km), or D ($\delta d > 30$ km). We herein limit our analysis to events of level A. Statistically, there are a

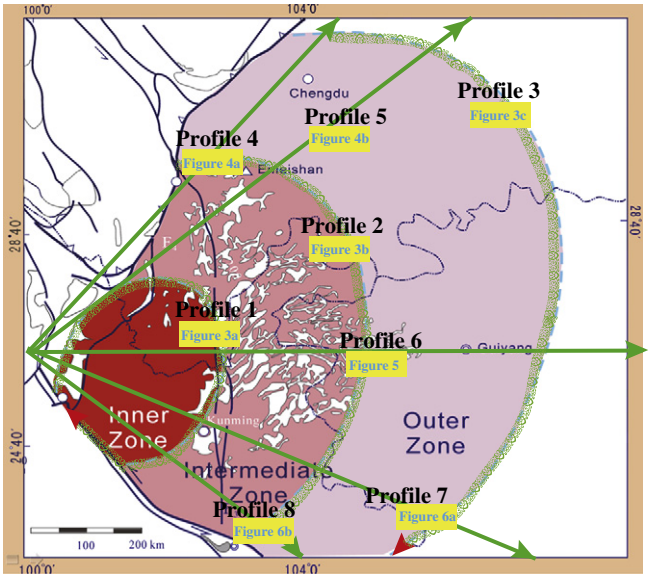

Fig. 2. ELIP profile distribution with three circular or semi-circular profiles, 1 (Fig. 3a), 2 (Fig. 3b), 3 (Fig. 3c), and five radial profiles, 4 (Fig. 4a), 5 (Fig. 4b), 6 (Fig. 5), 7 (Fig. 6a), and 8 (Fig. 6b).

total of 37,757 seismic events recorded within the scope of 100°–110°E, 22°–32°N, and there are 18,518 seismic events with depth parameters in the same area. The abilities of seismic location could be different for different periods, and even not quite accurate during the earlier period; however, the main trend of the focal depth distribution is not obviously changed. Thus, the uncertainty of the hypocenters of some events does not affect the understanding of the evolution of the ancient Emeishan mantle plume.

We used the catalog from CENC during the 1980–2010 period, and, using the relation of Richter $\mathrm{Log}E = 1.5Ms + 11.4$ (Richter, 1958) for each cell, we computed the total energy released by the earthquakes, grouping hypocenters in 4-km intervals. The value of *Ms* is either directly taken from the CENC catalog or computed from currently available relationships between *Ms* and M_L. As the focal depths did not exceed 60 km, the lower limit of the event depth distribution is 60 km (Figs. 3–6). The earthquake distribution versus depth is shown at the second row for each cell in Figs. 3–6. The earthquake energy distribution versus depth (Log*E*-h) is shown at the third row for each cell in Figs. 3–6. The logarithm of the energy for the grouped hypocenters was normalized to the maximal value $\log E_{max}$ for each cell, which is labeled as Log*E*/max(Log*E*), and the max(Log*E*) of each cell is marked at the bottom of each cell.

Figs. 3–6 show the seismic rheology and lithospheric structure of eight profiles, in which there are three profiles in a circle or semi-circle (Fig. 3), and there are five radial profiles (Figs. 4–6).

3.2. Lithosphere structure from deep seismic sounding

Lithosphere structure can provide important constraints on the deformation from a mantle plume. Numerous studies of mantle plumes: the Deccan traps in India, the Siberian traps of Asia, the Karoo–Ferrar basalts/dolerites in South Africa, Antarctica, the Paraná and Etendeka traps in South America and Africa (formerly a single province separated by opening of the South Atlantic Ocean), and the Columbia River basalts of North America all show the common feature that the crust beneath mantle plume will be thinned. When a plume head encounters the base of the lithosphere, it is expected to flatten out against this barrier and undergo widespread decompression melting to form large volumes of basalt magma. The plume head may then erupt onto the surface. Numerical modeling predicts that melting and eruption will occur over

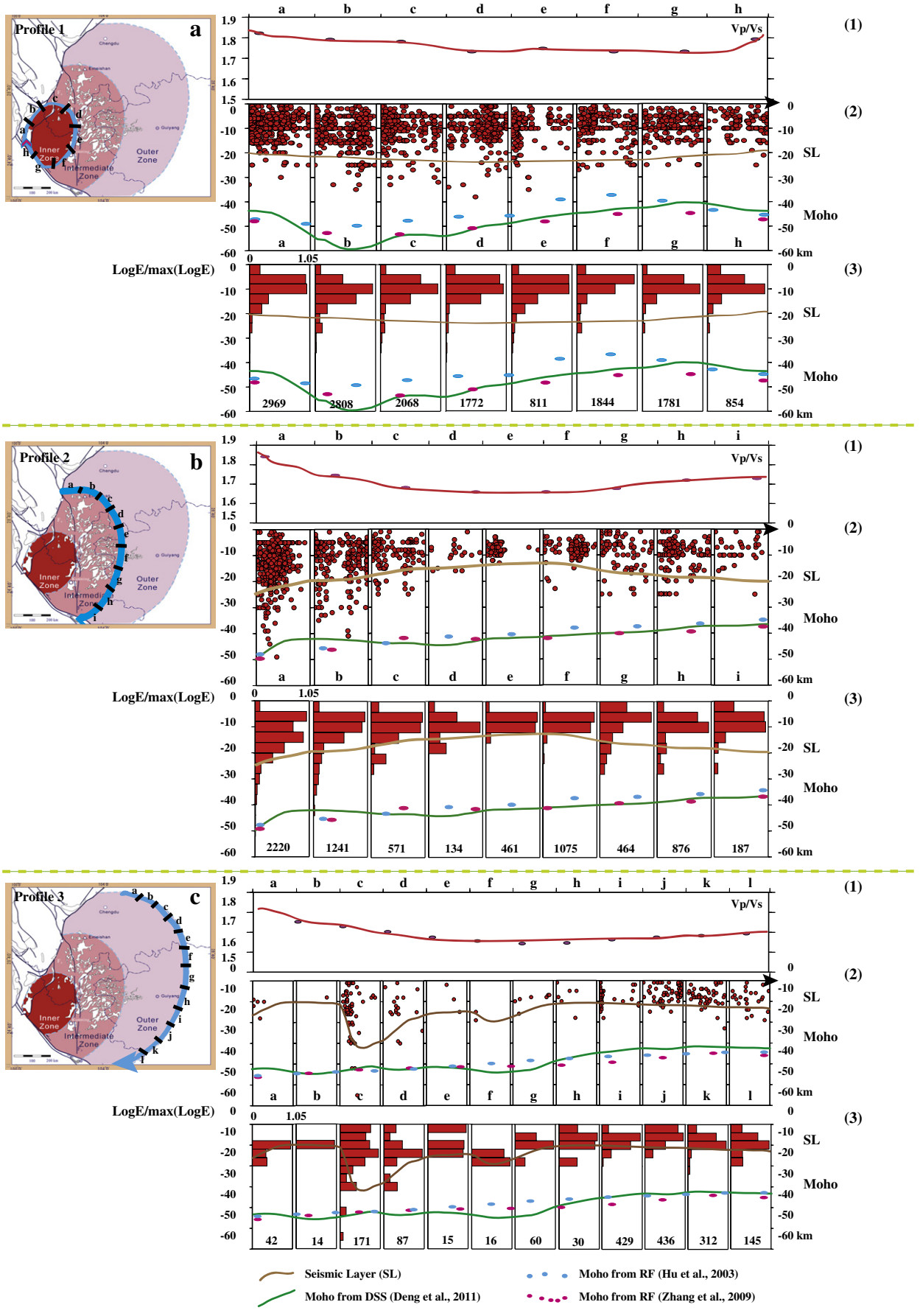

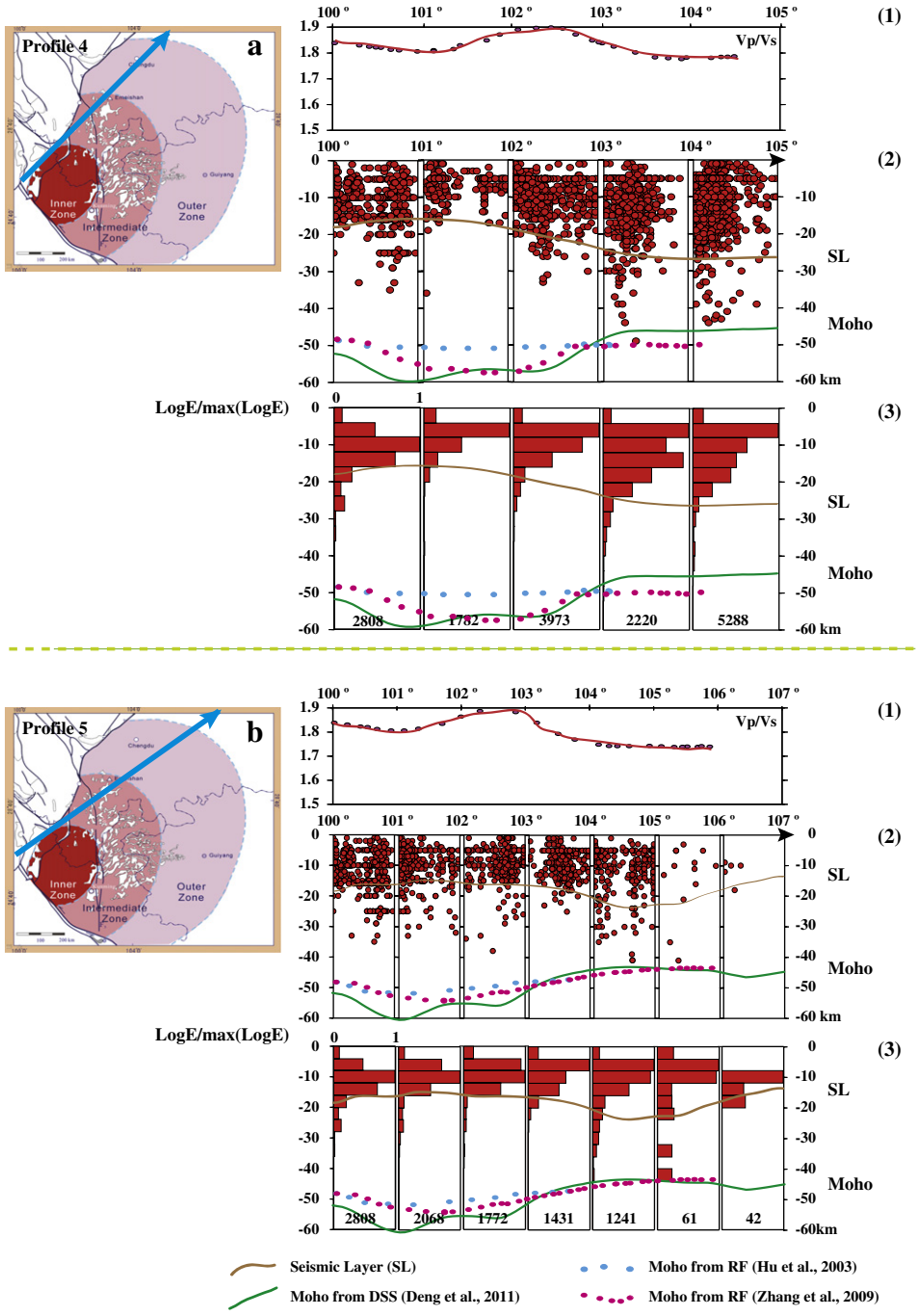

Fig. 4. a: On the left of the figure is a map showing the location of profile 4; the others are the same as Fig. 3a. b: On the left of the figure is a map showing the location of profile 5; the others are the same as Fig. 3a.

several million years. These eruptions have been linked to flood basalts, although many of these erupt over much shorter time scales (less than 1 million years). The mantle plume and its interaction with the underlying lithosphere should be recorded in the lithosphere structure.

Seismic data provide insights into the nature of the lithosphere, particularly regarding the transition between the crust and upper mantle. Deep seismic sounding methods can provide velocity, Moho depth and LAB depth along the profiles. Since 1980, numerous wide-angle seismic profiling studies have been conducted to understand the relationship between the crust structure and earthquake occurrence in Yunnan (Zhang et al., 2005a, b, 2010a, b; Zhang and Wang, 2009; Bai et al., 2010b). Furthermore, seismic surface wave tomography (Li et al., 2008a, b; Lei et al., 2009) and receiver function imaging (Hu et al., 2003; Zhang et al., 2009a) have been carried out in the last 30 years. These results suggest that the crust thickness increases from the south to the north and that the crustal composition shows prominent heterogeneity in Yunnan.

Fig. 3. a: On the left of the figure is a map showing the location of profile 1, and the three rows beside the map are: 1) the Vp/Vs ratio; 2) seismic distributions; 3) seismic energy distributions normalized as LogEmax, the maximum energy is shown at the bottom of each sub-block. More details about the calculation of the Vp/Vs ratio, seismic distribution, and seismic energy are in the text. The seismic layer, Moho depth from DSS (Deng et al., 2011), and Moho depth from RF (Hu et al., 2003; Zhang et al., 2009a, b) are shown in different colors at the proper positions in each map. b: On the left of the figure is a map showing the location of profile 2; the others are the same as Fig. 3a. c: On the left of the figure is a map showing the location of profile 3; the others are the same as Fig. 3a.

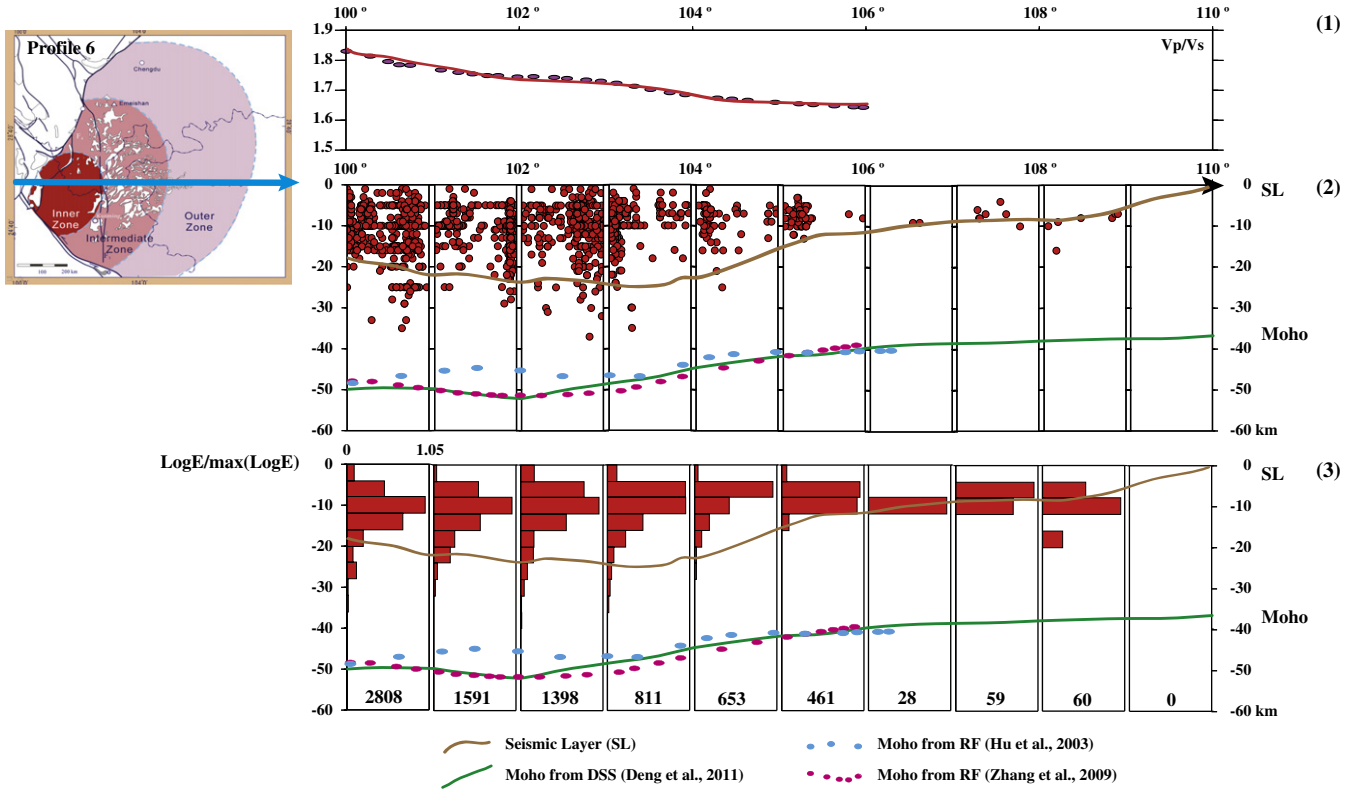

Fig. 5. On the left of the figure is a map showing the location of profile 6; the others are the same as Fig. 3a.

Here, we compile the crustal depth from 57 profiles (Cui et al., 1987; Xiong et al., 1993; Zhang et al., 2007; Deng et al., 2011). In addition, we used Moho depths obtained from receiver function imaging in south China (Hu et al., 2003; Zhang et al., 2009a). The Kriging method is used in the spatial interpolation of the Moho depth. The Kriging method provides an estimate of the error and confidence interval for every one of the unknown points, an asset not provided by other interpolation methods. Figs. 3–6 show that the spatial distribution of Moho depths from deep seismic sounding (Deng et al., in press) is consistent with that from receiver function imaging (Hu et al., 2003; Zhang et al., 2009a).

Here, we observe that the crustal thickness changes from approximately 60 km to 25 km in the whole ELIP. In detail, from Fig. 3a–c, the circular or semi-circular profiles show that the crustal thickness changes in the scope of 45–60 km at profile 1 (Fig. 3a), in the scope of 38–50 km at profile 2 (Fig. 3b), and in the scope of 35–45 km at profile 3 (Fig. 3c). The average crustal thickness change of the above three profiles is 12.3 km. In addition, from the five radial profiles (Figs. 4–6), it can be seen that the crustal thickness varies between 45 and 60 km at profile 4 (Fig. 4a), between 45 and 62 km at profile 5 (Fig. 4b), between 36 and 55 km at profile 6 (Fig. 5), between 25 and 55 km at profile 7 (Fig. 6a), and between 35 and 50 km at profile 8 (Fig. 6b). The average crustal thickness change of the above five profiles is 19.2 km. Comparing the averages of crustal thickness from the two kinds of profiles in the ELIP, it is seen that the crustal thickness change is much more prominent in the east–west direction than the north–south direction.

3.3. Crustal composition revealed by the Vp/Vs ratio and Poisson's ratio

The crustal composition is expected to vary systematically with the corresponding temperature decreasing from the inner zone to the outer zone of the mantle plume. Usually, both the Poisson's ratio and the Vp/Vs ratio can depict the physical and chemical state of the Earth so that the crustal composition can be predicted by either ratio (Christensen and Mooney, 1995; Zhang et al., 2009b). Experimental results show that the Poisson's ratio in the crust could be affected by geophysical and geochemical factors. The mineral constituents in the rock are quite influential on the change of Poisson's ratio (Tarkov and Vavakin, 1982; Christensen and Mooney, 1995). Similarly, Vp/Vs ratios can increase with the increasing degree of partial melting (Watanabe, 1993). Here, we evaluate the crustal composition from Vp/Vs ratio beneath the ELIP in the southeast margin of Tibet. The Vp/Vs ratio is derived from the H–K scanning of receiver functions beneath 25 temporary stations (23°–32°N, 97°–106°E) from one year's seismic records (Zhang et al., 2009a) with reference to the Moho depth and Poisson's ratio distribution in the similar research area beneath 23 permanent stations (21°–29°N, 97°–106°E) with three years' seismic records (Hu et al., 2003).

Fig. 7 displays the spatial distribution of average crustal Vp/Vs. Figs. 3–6 also show the radial and azimuthal variation of the average crustal Vp/Vs (the first column of Figs. 3–6). From these figures, we can observe that within 150 km of the center of the proposed mantle plume, the Vp/Vs ratio increases from 1.73 to 1.82. At a distance of 150–400 km from the suggested mantle plume center, the Vp/Vs ratio increases from 1.72 to 1.84, and 400–700 km from the proposed mantle plume center, the Vp/Vs ratio increases from 1.64 to 1.75 (Zhang et al., 2009a; Fig. 7). Beneath the mantle plume region, the crustal composition should display a systematic variation from beneath the plume head to its margins. From the receiver function imaging, the average Vp/Vs ratio or Poisson's ratio clearly decreases consistently with the distance from the center of the ELIP in the radial profiles in Figs. 4–6.

4. Discussion

4.1. Lateral variation of crustal thickness and seismogenic layer beneath the ELIP region

To estimate the crustal response and its possible modification to the mantle plume, we discuss the azimuthal and radial variations of

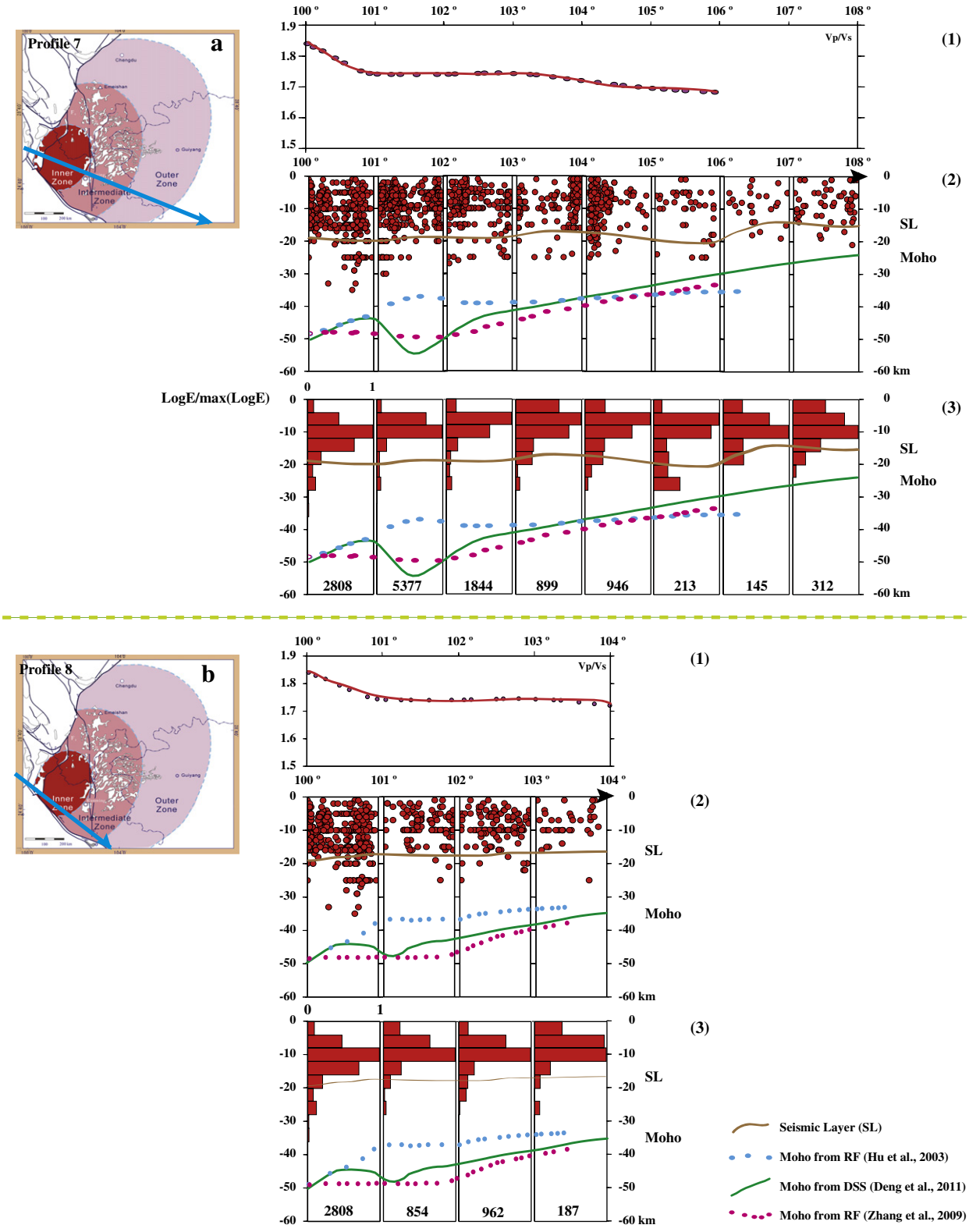

Fig. 6. a: On the left of the figure is a map showing the location of profile 7; the others are the same as Fig. 3a. b: On the left of the figure is a map showing the location of profile 8; the others are the same as Fig. 3a.

the lithosphere structure and seismic layer thickness beneath the ELIP. We discuss the azimuthal variation from three circular or semi-circular profiles in the inner, intermediate and outer zones as proposed by Xu et al. (2004) (Figs. 3a–c), and we discuss the radial variation from the five profiles extending from the inner to outer zones (Figs. 4–6). Along each profile, we estimate the seismogenic layer thickness (brittle layer), the seismic energy, and the Moho depths (Figs. 3–6).

4.1.1. Azimuthal variation of lithospheric structure and seismogenic layer

Figs. 3a–c display the azimuthal variation of lithospheric structure among the inner, intermediate, and outer zones of the ELIP. From the

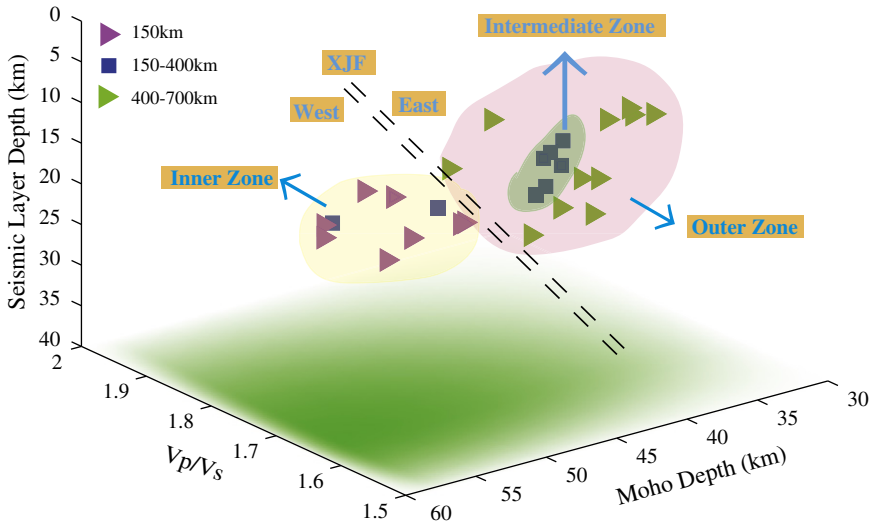

Fig. 7. The relationship of seismic layer depth, Vp/Vs ratio and Moho depth in Emeishan. The XJF is the Xiao Jiang Fault. The data in the inner zone (within 150 km of the proposed ELIP's center), the intermediate zone (within 150–400 km from the center of the proposed ELIP's center), and the outer zone (within 400–700 km from the center of the proposed ELIP's center) are marked in different colors.

studies of the Emeishan basalt, it is proposed that the crustal thickness is nearly constant in the azimuthal direction at the same distance from the center of the mantle plume (He et al., 2003; Xu et al., 2004). From Fig. 3a, the inner zone of the ELIP, the Moho depths range within 45–60 km, and the seismogenic layer ranges from 20 to 24 km. Correspondingly, the maximum focal depth is approximately 40 km,

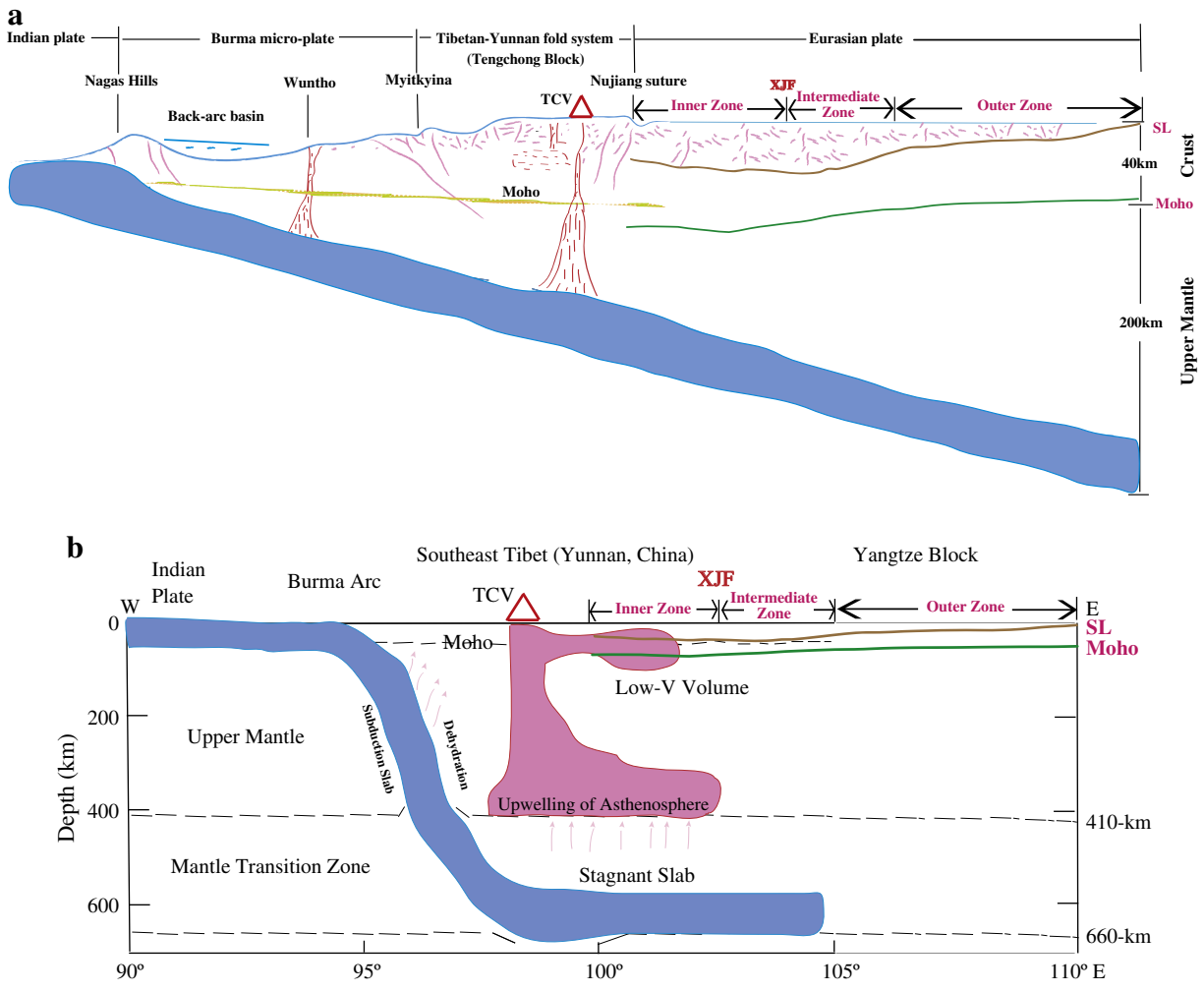

Fig. 8. The Indian Ocean plate eastward subduction models beneath southeast Tibet. Fig. 8a is the model updated from Wang and Gang, 2004, while Fig. 8b is updated from Lei et al., 2009. The Moho and seismic layers are from profile 6 and are marked with different colors.

most events occurred at 0–30 km, and the max(Log*E*) of the 4-km vertical interval is 2969 at the first cell. From Fig. 3b, the intermediate zone of the ELIP, the Moho depth is between 38 and 50 km, the seismogenic layer is between 12 and 24 km, the maximum focal depth is approximately 50 km at the first cell, most events occurred at 0–20 km, and the max(Log*E*) of the 4-km vertical interval is 2220 at the first cell, mainly caused by the Longmenshan Fault. From Fig. 3c, the outer zone of the ELIP, the Moho depth is between 35 and 45 km, the seismogenic layer is distributed between 10 and 24 km, and the maximum focal depth is approximately 60 km at the third column, most events occurred at 0–15 km, and the max(Log*E*) of the 4-km vertical interval is 436 at the tenth cell.

In the above three profiles (Fig. 3a–c), the Moho depth, the seismogenic layer, the focal depth, and the energy, they all decrease from west to the east (from the inner to the outer zone) of the ELIP. For the mantle plume, the focus area should be the hottest, and it should cool with distance from the focus area. Similarly, the seismic layer should be the shallowest under the focus area and should deepen with distance from the focus area, as should the Moho depth. In the ELIP, however, the common trend of the seismic layer and brittle crust cannot be observed. Rather, the inner zone shows the deepest, coldest and most brittle crust among the three zones, and the outer zone has a much more plastic nature. Thus, the Late Permian ELIP experienced some kind of prominent modifications after the Late Permian period, which resulted in the current, new brittle-plastic characteristics.

4.1.2. Radial variation of lithospheric structure and seismogenic layer

Figs. 4–6 illustrate the radial variation of the lithospheric structure and the seismogenic layer from the inner to the outer zones of the mantle plume. From Fig. 5, the profile that crosses the ELIP from west to east and from the inner zone to the outer zone directly shows that the Moho depth decreases from the inner zone to the outer zone (from 55 km to 36 km), the seismogenic layer from 24 km to 10 km, the focal depth from 40 km to 5 km, and the max(Log*E*) of the 4-km vertical interval from 2808 to 0. All of these decreases show that the Late Permian plume has radically changed.

Figs. 4 and 6 show the radial profiles of the lithospheric structure and seismogenic layer in different azimuth directions. Except for profile 4 (Fig. 4a), which passes through the Longmenshan thrust fault, all the other profiles show decreases in focal depth, Moho depth, and seismic energy from the inner zone to the outer zone, corresponding to the results from Figs. 3 and 5. The systematic variation of the seismogenic layer and the Moho depth suggests that the brittle layer decreases from the inner zone to outer zone of the postulated Emeishan mantle plume. However, the ductile layer thickens, which contradicts the expected variation trend of the brittle and ductile layers from the mantle plume: the brittle layer thickens from the inner to outer zone whereas the ductile layer thins from the inner to outer zone.

The Longmenshan Fault is located in the northwest border of the ELIP. The above seven profiles (excluding profile 4, Fig. 4a) demonstrate that the Late Permian ELIP developed into a new distribution since the Late Permian, resulting in the present brittle-plastic deformation. Figs. 3, 4b, 5, and 6 show that the focal depth and the energy decrease from the inner zone to the outer zone. A similar trend in brittle-plastic distribution is not shown in the northwestern border of the ELIP. It appears that the ELIP experienced some kind of prominent tectonically modifications since the Late Permian period, while the Longmenshan Fault (northwestern border of the ELIP) exhibits a different behavior from the whole ELIP.

4.2. The relationships among the seismogenic layer thickness, the Vp/Vs ratio and the Moho depth beneath the ELIP

The above discussion demonstrates that the mantle plume activity cannot explain our observation of radial/azimuthal variations of the seismogenic layer and the crustal thickness, which should represent the deformation from unclarified tectonic activities. To understand the modification of the mantle-plumed region, we summarize the lateral variation of crustal thickness (Zhang et al., 2009a), the average crustal Vp/Vs ratio (Zhang et al., 2009a) and the seismogenic layer thickness in the ELIP, as shown in Fig. 7. From the figure, we can observe that the XJF (*F6* in Fig. 1) acts as the boundary fault between the inner zone and the intermediate/outer zone. Tectonically, the XJF is a geologic border between the Middle-Yunnan and East-Yunnan blocks and is a gradient zone of the Moho depth, the Vp/Vs ratio, and the Poisson's ratio (Hu et al., 2003; Zhang et al., 2009a).

The following phenomenon can be observed from Fig. 7: within 150 km from the center of the proposed mantle plume, the crust thickens from 45 km to 53 km, the seismogenic layer thins slightly from 24 km to 20 km, and the Vp/Vs ratio increases from 1.73 to 1.82. Within a distance of 150–400 km from the suggested mantle plume center, the crust thins from 50 km to 38 km, the seismogenic layer thins from 24 km to 12 km, and the Vp/Vs ratio increases from 1.72 to 1.84. At 400–700 km from the proposed mantle plume center, the crust thins from 45 km to 34 km, the seismogenic layer thins from 24 km to 10 km, and the Vp/Vs ratio increases from 1.64 to 1.75.

In summary, crustal thickness has a positive correlation with the Vp/Vs ratio within 150 km of the center of the suggested mantle plume. However, there is a reverse correlation outside the central 150 km radius from the ELIP. The positive relation within 150 km of the ELIP center indicates that the Vp/Vs ratio increases with crustal thickening, which may have resulted from the addition of mafic materials from the mantle. The increases of both the crustal and seismic layer thicknesses from the center to the margin of the inner zone (Fig. 7) suggest that the mafic material from the mantle to the crust increases from the center to the outer margin of the inner circle, which may have resulted from the lateral flow of a basalt flood or from the fault (a channel of upwelling mafic material) at the outer margin of the inner circle. The first possibility suggests that the lithosphere structure beneath the inner circle of the speculated mantle plume can represent the result from mantle plume activity. The second possibility suggests that the lithosphere structure beneath the inner circle underwent the deformation from tectonic escape (Tapponnier et al., 1982). However, 150–700 km from the ELIP, the reverse correlation shows that the thinning crust corresponds to higher Vp/Vs ratios, which suggests that the middle crust beneath the ELIP could flow. The felsic middle crustal flow (with Vp/Vs less than 1.75) leads to crustal thinning and, consequently, an increasing average crustal Vp/Vs ratio. The middle crustal flow can be further supported from interpretation results of related wide-angle seismic profiling in the research area (Zhang et al., 2005a, b; Zhang and Wang, 2009) and the low electric resistance distribution in the middle crust from MT imaging (Bai et al., 2010a).

4.3. Understanding the thickness relationship between the crust and seismic layer

The Late Permian Emeishan mantle plume was proposed by Xu et al. (2004) (with the spatial distribution of the Emeishan mantle plume as shown in Fig. 1) and is divided into the inner, intermediate and outer zones of the plume (Xu et al., 2004). Numerous studies have demonstrated that a mantle plume can be characterized by high heat flow, active volcanism, variable topographic height depending on plume depth, and hotspot tracks with the age of magmatism and deformation increasing with distance from a hotspot (Condie, 2001). With the mantle plume model in our studied area, the lithosphere and crust should display systematic thickening from the inner zone to the intermediate and outer zones. Correspondingly, the temperature should decrease from the inner to outer zones. The lithospheric rheology structure should have a consistent pattern with lithosphere thickness or crustal thickness, which means the

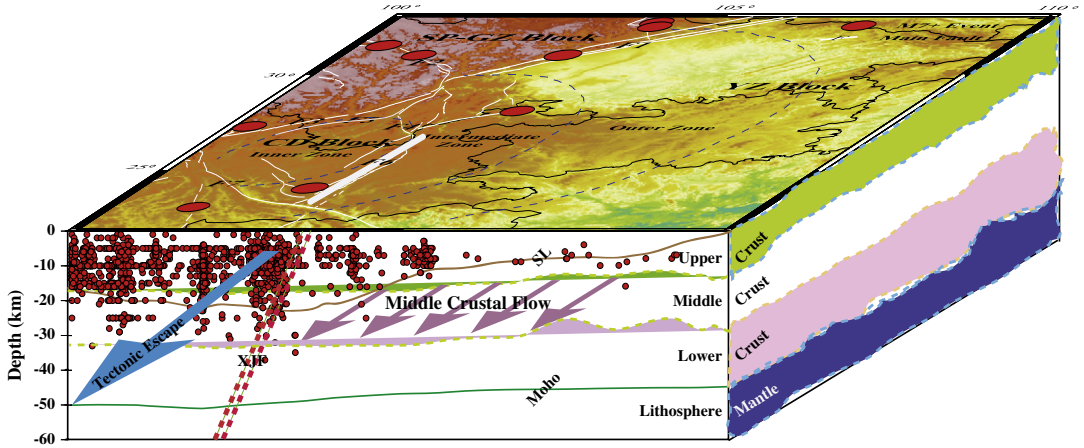

Fig. 9. The geodynamic model beneath the ELIP. The tectonic escape at the west of the XJF and the north-southward middle crustal flow at the east of the XJF (to the Late Permian mantle plume); the earthquake distribution is from profile 6 (Fig. 5).

brittle layer thickness of the lithosphere should be the thinnest beneath the central zone and the thickest beneath the outer zone.

The studied area is approximately 100 km east of the Tengchong volcano (TCV in Fig. 8a and b). We can observe that between the TCV and XJF (in the inner zone of the Late Permian Emeishan mantle plume), the seismogenic layer maintains an approximately 20-km thickness with slight thickening whereas the aseismic layer (ductile layer) in the crust remains at a relatively constant 30 km (Fig. 8a and b). Further eastward from the XJF (from the intermediate to the outer zone of the proposed Late Permian Emeishan mantle plume), we find the seismogenic layer thins from 24 km to 0 km (Fig. 8a and b) whereas the ductile layer thickens from 24 to 38 km. The lithospheric rheology structure in the present form may not support the existence of the mantle plume centered at the proposed inner zone (Figs. 1, 8a and b) and may have undergone successive deformations, such as deformation from the eastward subduction of the Indian Ocean plate or from the nearly north-southward tectonic escape/crustal flow. The later deformation to the lithosphere structure beneath the mantle plume should have different modification mechanisms in the inner and intermediate/outer zones.

Our observations of the crustal thickness and seismogenic layer (Figs. 3–6) confirm this general relationship between the crustal thickness and seismogenic layer thickness beneath the Emeishan mantle plume, which may have resulted from the successive deformation of the following geodynamic activities, such as the eastward subduction of the Indian Ocean plate or the southward tectonic escape/crustal flow to accommodate the collision between the Indian and Eurasian plates. This successive modification to the mantle plume may be supported by geochemical observations that require complexity in this simple thermal-zonation model. Specifically, within the inner zone sections, high-Ti-HT1 and HT2–HT3-lavas occur in the uppermost sequence of evolved alkaline lava (hawaiite to phonolite) between the high-Ti lavas in the Miyi section. These high-Ti and alkaline lavas may be relatively young compared with low-Ti lavas and may reflect the waning of plume-related volcanism (Xu et al., 2001). Low-Ti, HT2–HT3, and alkaline lavas occur exclusively in the inner zone, and they were subject to significant crustal contamination (Xu et al., 2001). These factors may be largely related to the thermal remobilization of the lithosphere above the plume head compared with that above the plume periphery (Xu et al., 2004).

4.3.1. Eastward subduction of the Indian Ocean plate?

Tectonically, the studied region is closely related to the eastward subduction of the Indian Ocean plate compared with the nearly northward subduction of Indian plate beneath the Himalayas (Hirn et al., 1984; Teng et al., 1985; Zhao et al., 1993; Makovsky et al., 1996; Zhang and Klemperer, 2010). The spatial distribution of earthquake foci from the International Seismological Catalogue (ISC) shows the earthquake belt as an eastward-dipping belt beneath Burma (Verma et al., 1980; Zhang and Zang, 1986). Geochemical and isotopic data show that the main (most voluminous) series of lavas were derived by partial melting of a metasomatized and heterogeneous mantle source, with crustal and possibly seawater components probably related to the previous subduction beneath Asia (Zhu et al., 1983). The content of Rb and Sr and other geochemical data suggest that these volcanic rocks belong to the high-K calc-alkaline series of magma formed in the collision zone (Mu et al., 1987). The Cenozoic TCV activity shows the geochemical features of island-arc or active continental margins (Cong et al., 1994).

TCV and the other deepening patterns of earthquake occurrence are attributed to oceanic plate subduction. There are two kinds of models: one (Fig. 8a) is based on interpretational results of the deep seismic sounding profiles (Wang and Gang, 2004; Zhang et al., 2005a, b; Zhang and Wang, 2009) and another (Fig. 8b) is proposed from local and teleseismic travel time tomography (Li et al., 2008a, b; Lei et al., 2009). In the first case (Fig. 8a), the volcanic activities beneath Burma and TCV are attributed to the dehydration fluid processing from the subducted Indian Ocean plate (Wang and Gang, 2004). In the model, the Indian Ocean plate subducts with a constant slip angle to a depth of approximately 200 km beneath the Nujiang Suture. In the second case (Fig. 8b), the volcanic activity beneath the Burma arc and the TCV are derived from different depths of seismic sources (Lei et al., 2009). In the model, the Indian Ocean plate horizontally subducts beneath the Burma arc and then turns to steepen slowly to the mantle transition zone, acting as a stagnant slab in the MTZ beneath the western margin of southeast Tibet. The Burma arc volcanic activity is directly related to the dehydration of the subducted Indian Ocean plate, and the TCV activity is related to the upwelling of asthenosphere at a depth of 410 km heated by the stagnant slab.

Figs. 4–6 show that the Vp/Vs ratio decreases gradually along the profiles. Furthermore, the Moho depth and seismogenic depth both gently thin. Fig. 8b shows a sharp subduction angle beneath the Burma arc, which could result in the response of the crustal composition or velocity structures; however, we do not observe similar sharp changes in the Vp/Vs ratio, the Moho depth, or the seismogenic depth. Both models in Fig. 8a and b should lead to the thickening of the ductile layer, at least in the inner zone, which conflicts with our observations. Thus, we speculate that our results of lithosphere rheology in the studied area may suggest that the Indian Ocean plate subduction does not provide a strong contribution to the deformation superposed upon the mantle plumed lithosphere.

4.3.2. Southward tectonic escape or crustal flow?

Several major strike–slip faults are present on the Tibetan Plateau, including the Altyn Tagh, Kunlun, Xianshuihe, Jiali, Red River, and Karakoram fault systems. In eastern Tibet, left-and right-lateral faults translate Tibetan terranes eastward, although the magnitudes of translation versus rotation and distributed motion are still debated (Tapponnier et al., 1982, 1990; Yin and Harrison, 2000; Wang et al., 2001). The left-lateral Altyn Tagh Fault, which forms the northwestern boundary of the Tibetan Plateau, has accommodated a 280–550 km (Peltzer and Tapponnier, 1988; Yin and Harrison, 2000) or 375 ± 25 km (Yue et al., 2001) slip since the Oligocene.

The studied area is located at the northeastern edge of the collision zone between the Indian and Eurasian plates. The long-distance tectonic escape of large crustal fragments accommodated by strike–slip faulting is required by the rigid indentation model (Tapponnier et al., 1982) compared with models that require mantle dynamics, including lamination-induced isostatic rebound in combination with crustal thickening by pure shear (Molnar et al., 1993) and models that inflate the crust by significant amounts of magmatic underplating (Powell and Conaghan, 1973; Molnar, 1988; Bird, 1991). The tectonic escape model has been supported by recent studies of the geology of the Tibetan Plateau and by neotectonic studies of fault slip rates, even though the actual amounts of lateral escape versus distributed shortening and rotation are still debated (Yin and Harrison, 2000). Yunnan (at the southeast margin of Tibetan plateau) is the key area influenced by tectonic escape (Tapponnier et al., 1982) or crustal flow (Royden et al., 1997; Zhang and Wang, 2009; Bai et al., 2010a; Chen et al., 2010; Zhang and Klemperer, 2010).

From Fig. 7, we observe the distinctive difference of crustal properties between the west and east of the XJF. In the west of the fault, the crustal thickness has a positive correlation with the Vp/Vs ratio within 150 km of the center of the suggested mantle plume. However, there is a reverse correlation in the east of the fault outside of the central 150 km scope in the ELIP.

The thinning seismogenic layer and the thickening ductile layer in the crust beneath the intermediate/outer zones of the ELIP and the relatively constant seismogenic and ductile layers beneath the inner zone of the ELIP (Fig. 5) hint that the geodynamic models could be different in the east and west of the XJF, the border between the inner and intermediate/outer zones. The positive relation within 150 km in the inner zone may have resulted with the lateral flow of basaltic flooding or from the fault (a channel of upwelling of mafic material) at the outer margin of the inner circle. However, 150–700 km from ELIP, the reverse correlation shows that the thinning crust corresponds to higher Vp/Vs ratios, which suggests that the middle crust beneath the ELIP could flow. The above inference is consistent with our observation of the lateral/azimuthal variation of the seismogenic layer. Our results allow us to postulate that the ELIP (the Late Permian mantle plume) endured successive deformation from the north-southward tectonic escape beneath the west of the XJF and from the middle crustal flow beneath the east of the XJF (Fig. 9).

5. Conclusion

In this paper, we obtain three kinds of geophysical results: (1) seismicity from events recorded and located by permanent seismic networks, (2) crustal structure from deep seismic sounding, and (3) crustal composition structure from receiver function imaging. Our results demonstrate that the seismogenic (brittle) layer thins away from the proposed center of the Emeishan mantle plume (approximately 24 km in depth beneath the center of Emeishan mantle plume and only approximately 10 km in depth beneath the margin of the plume), and the aseismic (ductile) layer thickens from the proposed center of the Emeishan mantle plume (relatively constant in thickness beneath the inner zone of the ELIP approximately 24 km, increasing in thickness from 24 km to 38 km beneath the intermediate/outer zones of the ELIP). Correspondingly, the crustal thickness decreases from the inner zone to the outer zone. The average crustal Vp/Vs ratio increases at three zones.

Seismological studies mentioned above support that the lithospheric structure and rheology of the Permian Emeishan mantle plume have tectonically modified during Mesozoic–Cenozoic. Furthermore, the thinning seismogenic layer and the thickening ductile layer in the crust beneath the intermediate/outer zones of the ELIP and the relatively constant seismogenic and ductile layers beneath the inner zone of the ELIP mean that the tectonic models could be different in the east and west of the XJF, the border between the inner and intermediate/outer zones. Considering the geologic and geochemistry observations in ELIP and its adjacent area, these remarkable features are interpreted as the modification of tectonic escape at the west of the XJF and a north-southward middle crust flow at the east of the XJF (to the Late Permian mantle plume).

Acknowledgments

This study is financially supported by National Basic Research Program of China (973 Program, grant 2011CB808904), National Natural Science Foundation of China (grants 41021063, 41074037, 40804012, and 41090292), and the Special Research Project in Earthquake Science, China Earthquake Administration (grant 200808068). The paper has benefited a lot from the constructive suggestions of Professor M. Santosh, Professor Alan Aitken, and two anonymous reviewers.

References

Ali, J.R., Thompson, G.M., Song, X., Wang, Y., 2002. Emeishan basalts (SW China) and the "end-Guadalupian" crisis: magnetobiostratigraphic constraints. Journal of the Geological Society of London 159, 21–29.

Bai, D.H., Unsworth, M.J., Meju, M.A., Ma, X.B., Teng, J.W., Kong, X.R., Sun, Y., Sun, J., Wang, L.F., Jiang, C.S., Zhao, C.P., Xiao, P.F., Liu, M., 2010a. Crustal deformation of the eastern Tibetan plateau revealed by magnetotelluric imaging. Nature Geoscience. doi:10.1038/NGEO830.

Bai, Z.M., Tian, X.B., Tian, Y., 2010b. Upper mantle P-wave tomography across the Longmenshan Fault belt from passive-source seismic observations along Aba–Longquanshan profile. Journal of Asian Earth Sciences 40, 873–882.

Bird, P., 1991. Lateral extrusion lower crust from under high topography in the isostatic limit. Journal of Geophysical Research 96, 10 275–10 286.

Campbell, I.H., Griffiths, R.W., 1990. Implications of mantle plume structure for the evolution of flood basalts. Earth and Planetary Science Letters 99, 79–93.

Chen, Y., Badal, J., Hu, J.F., 2010. Love and Rayleigh wave tomography of the Qinghai–Tibet Plateau and surrounding areas. Pure and Applied Geophysics 167, 1171–1203.

Chen, C.H., Hsieh, P.S., Lee, C.Y., Zhou, H.W., 2011. Two episodes of the Indosinian therman event on the South China Block: constraints from LA–ICPMS U–Pb zircon and electron microprobe monazite ages of the Darongshan S-type granitic suite. Gondwana Research 19, 1008–1023.

Cheng, S.H., Kusky, T., 2007. Komatiites from west Shandong, North China craton: implications for plume tectonics. Gondwana Research 12, 77–83.

Christensen, N.I., Mooney, W.D., 1995. Seismic velocity structure and composition of the continental crust: a global view. Journal of Geophysical Research 100, 9761–9788.

Chung, S.L., Jahn, B.M., 1995. Plume–lithosphere interaction in generation of the Emeishan flood basalts at the Permian–Triassic boundary. Geology 23, 889–992.

Chung, S.L., Lee, T.Y., Lo, C.H., Wang, P.L., Chen, C.Y., Nguyen, T.Y., Tran, T.H., Wu, G.Y., 1997. Intraplate extension prior to continental extrusion along the Ailao Shan–Red River shear zone. Geology 25, 311–314.

Chung, S.L., Jahn, B.M., Wu, G.Y., Lo, C.H., Cong, B.L., 1998. The Emeishan flood basalt in SW China: a mantle plume initiation model and its connection with continental break-up and mass extinction at the Permian–Triassic boundary. In: Flower, M.F.J., Chung, S.L., Lo, C.H., Lee, T.Y. (Eds.), Mantle Dynamics and Plate interaction in East Asia: AGU Geodynamic Series, 27, pp. 47–58.

Clark, M.K., Royden, L.H., 2000. Topographic ooze: building the eastern margin of Tibet by lower crustal flow. Geology 28, 703–706.

Condie, K., 2001. Mantle Plumes and their Record in Earth History. Cambridge University Press, Cambridge, UK. 306 pp.

Cong, B.L., Chen, Q.Y., Zhang, R.Y., Wu, G.Y., Xu, P., 1994. Origin of Tengchong Cenozoic volcanic rocks in western Yunnan. China. Science in China Series B: Chemistry 24, 441–448 (in Chinese).

Courtillot, V.E., Renne, P.R., 2003. On the ages of flood basalt events. Comptes Rendus Geosciences 335, 113–140.

Cui, Z.Z., Lu, D.Y., Chen, J.P., Zhang, Z.Y., Huang, L.Y., 1987. The deep structure and tectonic features of the crust in Panxi area. Chinese Journal of Geophysics 30 (2), 566–580 (in Chinese with English abstract).

Deng, Y.F., Li, S.L., Fan, W.M., Liu, J., 2011. Crustal structure beneath South China revealed by deep seismic soundings and its dynamics implications. Chinese Journal of Geophysics 54 (10), 2560–2574.
Ernst, W.G., 2006. Speculations on evolution of the terrestrial lithosphere–asthenosphere system—plumes and plates. Gondwana Research 11, 38–49.
Geiger, L., 1912. Probability method for the determination of earthquake epicentres from arrival time only. Bulletin of Saint Louis University 8, 60–71.
Goes, S., Spakman, W., Bijwaard, H., 1999. A lower mantle source for central European volcanism. Science 286, 1928–1931.
Hanski, E., Walker, R.J., Huhma, H., Polyakov, G.V., Balykin, Hoa T.T., Phuong, N.T., 2004. Origin of the Permian–Triassic komatiites, north-western Vietnam. Contributions to Mineralogy and Petrology 147, 453–469.
He, B., Xu, Y.G., Chung, S.L., Xiao, L., Wang, Y., 2003. Sedimentary evidence for a rapid crustal doming prior to the eruption of the Emeishan flood basalts. Earth and Planetary Science Letters 213, 389–403.
Hirn, A., Lepine, J.C., Jobert, G., Sapin, M., Wittlinger, G., Xu, Z.X., Gao, E.Y., Wang, X.J., Teng, J.W., Xiong, S.B., Pandey, M.R., Tater, J.M., 1984. Crustal structure and variability of Himalayan border of Tibet. Nature 307, 23–25.
Hu, J.F., Su, Y.J., Zhu, X.G., Chen, Y., 2003. Crustal Vs, Poisson's ratio structures and significances. Science in China Series D: Earth Sciences 33 (8), 714–722 (in Chinese).
Klein, W., 2002. User's guide to hypoinverse-2000, a Fortran program to solve for earthquake locations and magnitudes. U.S. Geological Survey, open file report 02–171.
Lei, J.S., Zhao, D.P., 2006. A new insight into the Hawaiian plume. Earth and Planetary Science Letters 241, 438–453.
Lei, J.S., Zhao, D.P., Su, Y.J., 2009. Insight into the origin of the Tengchong intraplate volcano and seismotectonics in southwest China from local and teleseismic data. Journal of Geophysical Research 114, B05302 1–18.
Li, X., Kind, R., Priestley, K., Sobolev, S., Tilmann, F., Yuan, X., Weber, M., 2000. Mapping the Hawaiian plume conduit with converted seismic waves. Nature 405, 938–941.
Li, C., van der Hilst, R.D., Meltzer, A.S., Engdahl, E.R., 2008a. Subduction of the Indian lithosphere beneath the Tibetan Plateau and Burma. Earth and Planetary Science Letters 274, 157–168.
Li, Y., Wu, Q., Zhang, R., Tian, X., Zeng, R., 2008b. The crust and upper mantle structure beneath Yunnan from joint inversion of receiver functions and Rayleigh wave dispersion data. Physics of the Earth and Planetary Interiors 170, 134–146.
Lo, C.H., Chung, S.L., Lee, T.Y., Wu, G.Y., 2002. Age of the Emeishan flood magmatism and relations to Permian–Triassic boundary events. Earth and Planetary Science Letters 198, 449–458.
Makovsky, Y., Klemperer, S.L., Huang, L.Y., Lu, D.Y., Project Indepth Team, 1996. Structural elements of the southern Tethyan Himalaya crust from wide-angle seismic data. Tectonophysics 15, 997–1005.
McKenzie, D.P., O'Nions, R.K., 1991. Partial melt distributions from inversion of rare earth element concentrations. Journal of Petrology 32, 1021–1091.
Molnar, P., 1988. A review of geophysical constraints on the deep structure of the Tibetan plateau, the Himalaya, and the Karakoram, and their implications. Philosophical Transactions of the Royal Society London A 326, 33–88.
Molnar, P., Tapponnier, P., 1975. Tectonics in Asia: consequences and implications of a continental collision. Science 189, 419–426.
Molnar, P., England, P., Martinod, J., 1993. Mantle dynamics, uplift of the Tibetan Plateau, and the Indian Monsoon. Reviews of Geophysics 31, 357–396.
Montelli, R., Nolet, G., Dahlen, F.A., Masters, G., Engdahl, E.R., Hung, S.H., 2004. Finite-frequency tomography reveals a variety of plumes in the mantle. Science 303 (5656), 338–343.
Montelli, R., Nolet, G., Dahlen, F.A., Masters, G., 2006. A catalogue of deep mantle plumes: new results from finite-frequency tomography. Geochemistry, Geophysics, Geosystems 7, Q11007 69 pp.
Mu, Z.G., Tong, W., Curtis, G.H., 1987. Timing of Tengchong volcanic activities and related magmatic source. Acta Geophysica Sinica 30 (3), 261–270 (in Chinese).
Panza, G.F., Raykova, R.B., 2008. Structure and rheology of lithosphere in Italy and surrounding. Terra Nova 20, 194–199.
Peltzer, G., Tapponnier, P., 1988. Formation and evolution of strike–slip faults, rifts, and basins during the India–Asia collision: an experimental approach. Journal of Geophysical Research 93, 15 085–15 117.
Powell, C.M., Conaghan, P.J., 1973. Plate tectonics and the Himalayas. Earth and Planetary Science Letters 20, 1–12.
Rhodes, M., Davies, J.H., 2001. Tomographic imaging of multiple mantle plumes in the uppermost lower mantle. Geophysical Journal International 147, 88–92.
Richter, C.F., 1958. Elementary Seismology. W.H.Freeman and Co., San Francisco.
Ritsema, J., Allen, R.M., 2003. The elusive mantle plume. Earth and Planetary Science Letters 207, 1–12.
Romanowicz, B., Gung, Y., 2002. Superplumes from the core–mantle boundary to the lithosphere: implications for heat flux. Science 296, 513–516.
Roy, A., Sarkar, A., Jeyakumar, S., Aggrawal, S.K., Ebihara, M., 2002. Mid-Proterozoic plume-related thermal event in Eastern Indian Craton: evidence from trace elements, REE geochemistry and Sr–Nd isotope systematics of basic–ultrabasic intrusives from Dalma volcanic belt. Gondwana Research 5, 133–146.
Royden, L.H., Burchfiel, B.C., King, R.W., Chen, Z., Shen, F., Liu, Y., 1997. Surface deformation and lower crustal flow in eastern Tibet. Science 276, 788–790.
Su, B.X., Qin, K.Z., Sakyi, P.A., Li, X.H., Yang, Y.H., Sun, H., Tang, D.M., Liu, P.P., Xiao, Q.H., Malaviarachchi, S.P.K., 2011. U–Pb ages and Hf–O isotopes of zircons from Late Paleozoic mafic–ultramafic units in the southern Central Asian Orogenic Belt: tectonic implications and evidence for an Early-Permian mantle plume. Gondwana Research 20, 516–531.
Tapponnier, P., Peltzer, G., Le Dain, A.Y., Armijo, R., Cobbold, P., 1982. Propagating extrusion tectonics in Asia: new insights from simple experiments with plasticine. Geology 10, 611–616.
Tapponnier, P., Lacassin, R., Leloup, P.H., Scharer, U., Zhong, D.L., Wu, H.W., Liu, X.H., Ji, S.C., Zhang, L.S., Zhong, J.Y., 1990. The Ailao Shan–Red River metamorphic belt: Tertiary left-lateral shear between Indochina and South China. Nature 343, 431–437.
Tarkov, A.P., Vavakin, V.V., 1982. Poisson's ratio behaviour in crystalline rocks: application to the study of the Earth's interior. Physics of the Earth and Planetary Interiors 29, 24–29.
Teng, J.W., Xiong, S.B., Yin, Z.X., 1985. Seismic velocity distribution and crustal velocity in Xizang (Tibet) Plateau. Chinese Journal of Geophysics 28 (1), 16–27 (in Chinese with English abstract).
Verma, R.K., Mukhopadhyay, M., Nag, A.K., 1980. Seismicity and tectonics in South China and Burma. Tectonophysics 64, 85–96.
Waldhauser, F., Ellsworth, W.L., 2000. A double-difference earthquake location algorithm: method and application to the northern Hayward Fault California. Bulletin of the Seismological Society of America 90, 1353–1368.
Wang, C.Y., Gang, H.F., 2004. Crustal structure in Tengchong volcano-geothermal area, western Yunnan, China. Tectonophysics 380, 69–87.
Wang, J., Yin, A., Harrison, T., Grove, M., Zhang, Y., Xie, G., 2001. A tectonic model for Cenozoic igneous activities in the eastern Indo–Asian collision zone. Earth and Planetary Science Letters 188, 123–133.
Wang, X.C., Li, X.H., Li, W.X., Li, Z.X., 2009. Variable involvements of mantle plumes in the genesis of mid-Neoproterozoic basaltic rocks in South China: a review. Gondwana Research 15, 381–395.
Watanabe, T., 1993. Effects of water and melt on seismic velocities and their application to characterization of seismic reflectors. Geophysical Research Letters 20, 2933–2936.
Whitehead, J.A., Luther, D.S., 1975. Dynamics of laboratory diaper and plume models. Journal of Geophysical Research 80, 705–717.
Wignall, P.B., Sun, Y.D., Bond, D.P.G., Izon, G., Newton, R.J., et al., 2009. Volcanism, mass extinction, and carbon isotope fluctuations in the Middle Permian of China. Science 324, 1179–1182.
Xiao, L., Xu, Y.G., Chung, S.L., He, B., Mei, H.J., 2003. Chemostratigraphic correlation of Upper Permian lava succession from Yunnan province, China: extent of the Emeishan Large Igneous Province. International Geology Review 45, 753–766.
Xiong, S.B., Zheng, Y., Yin, Z.X., Zeng, X.X., Quan, Y.L., Sun, K.Z., 1993. The 2-D structure and its tectonic implications of the crust in the Lijiang–Panzhihua–Zhehai region. Chinese Journal of Geophysics 36 (4), 434–444 (in Chinese with English abstract).
Xu, Y.G., Chung, S.L., Jahn, B.M., Wu, G.Y., 2001. Petrologic and geochemical constraints on the petrogenesis of Permian–Triassic Emeishan flood basalts in southwestern China. Lithos 58, 145–168.
Xu, Y.G., He, B., Chung, S.L., Menzies, M.A., Frey, F.A., 2004. The geologic, geochemical and geophysical consequences of plume involvement in the Emeishan flood basalt province. Geology 30, 917–920.
Xu, Y.G., He, B., Huan, X.L., Luo, Z.Y., Chung, S.L., Xiao, L., Zhu, D., Shao, H., Fan, W.M., Xu, J.F., Wang, Y.J., 2007. Identification of mantle plumes in the Emeishan Large Igneous Province. Episodes 30, 32–42.
Yin, A., Harrison, T.M., 2000. Geologic evolution of the Himalayan–Tibetan orogen. Annual Review of Earth and Planetary Sciences 28, 211–280.
Yu, X., Yang, S.F., Chen, H.L., Chen, Z.Q., Li, Z.L., Batt, G.E., Li, Y.Q., 2011. Permian flood basalts from the Tarim Basin, Northwest China: SHRIMP zircon U–Pb dating and geochemical characteristics. Gondwana Research 20, 485–497.
Yue, Y., Ritts, B.D., Graham, S.A., 2001. Initiation and long-term slip history of the Altyn Tagh Fault. International Geology Review 43, 1087–1093.
Yuen, D., Cadek, O., Chopelas, A., Matyska, C., 1993. Geophysical inferences of thermal–chemical structures in the lower mantle. Geophysical Research Letters 20, 899–902.
Zhang, Z.J., Klemperer, S., 2010. Crustal structure of the Tethyan Himalaya, southern Tibet: new constraints from old wide-angle seismic data. Geophysical Journal International 181, 1247–1260.
Zhang, X., Wang, Y.H., 2009. Seismic velocity structure of crust and upper mantle in Yunnan, Southwestern China. Tectonophysics 471, 171–185.
Zhang, J., Zang, S., 1986. Characteristics of earthquake distribution and the mechanism of earthquakes in the boundary area between Burma, India and China. Acta Seismologica Sinica 8, 240–253 (in Chinese).
Zhang, Z.J., Bai, Z.M., Wang, C.Y., Teng, J.W., Lv, Q.T., Li, J.L., Liu, Y.F., Liu, Z.K., 2005a. The crustal structure under Sanjiang and its dynamic implications: revealed by seismic reflection/refraction profile between Zhefang and Binchuan, Yunnan. Science in China Series D: Earth Sciences 48 (9), 1329–1336.
Zhang, Z.J., Bai, Z.M., Wang, C.Y., Teng, J.W., Lv, Q.T., Li, J.L., Sun, S.X., Wang, X.Z., 2005b. Crustal structure of Gondwana and Yangtze typed blocks: an example by wide-wangle seismic profile from Menglian to Malong in Western Yunnan. Science in China Series D: Earth Sciences 48 (11), 1826–1836.
Zhang, Z.C., Mahoney, J.J., Mao, J.W., Wang, F.H., 2006. Geochemistry of picritic and associated basalt flows of the western Emeishan flood basalt province, China. Journal of Petrology 47, 1997–2019.
Zhang, Z., Xu, C.M., Meng, B.Z., Liu, C., Teng, J.W., 2007. Crustal reflectivity characters from the Eryuan–Jiangchuan wide-angle seismic profile. Chinese Journal of Geophysics 50 (4), 1082–1088 (in Chinese with English abstract).
Zhang, H.S., Tian, X.B., Teng, J.W., 2009a. Estimation of crustal Vp/Vs with dipping Moho from receiver functions. Chinese Journal of Geophysics 52 (5), 1243–1252 (in Chinese with English abstract).
Zhang, Z.J., Wang, Y.H., Chen, Y., Houseman, G.A., Tian, X.B., Wang, E.Q., Teng, J.W., 2009b. Crustal structure across Longmenshan Fault belt from passive source seismic profiling. Geophysical Research Letters 36, L17310. doi:10.1029/2009GL039580.
Zhang, Y.T., Liu, J.Q., Guo, Z.F., 2010a. Permian basaltic rocks in the Tarim basin, NW China: implications for plume–lithosphere interaction. Gondwana Research 18, 596–610.
Zhang, Z.J., Deng, Y.F., Teng, J.W., Wang, C.Y., Gao, R., Chen, Y., Fan, W., 2010b. An overview of the crustal structure of the Tibetan plateau after 35 years of deep seismic soundings. Journal of Asian Earth Sciences 40, 977–989.

Zhang, Z.J., Wu, J., Deng, Y.F., Teng, J.W., Chen, Y., Panza, G., submitted for publication. Lateral variation of lithosphere rheology structure across the eastern North China Craton: new constrains on its lithospheric disruption. Geophysics Journal International.
Zhao, D.P., 2001. Seismic structure and origin of hotspots and mantle plumes. Earth and Planetary Science Letters 192, 251–265.
Zhao, D.P., 2004. Global tomographic images of mantle plumes and subducting slabs: insight into deep Earth dynamics. Physics of the Earth and Planetary Interiors 146, 3–34.
Zhao, D.P., 2007. Seismic images under 60 hotspots: search for mantle plumes. Gondwana Research 12, 335–355.
Zhao, D.P., 2009. Multiscale seismic tomography and mantle dynamics. Gondwana Research 15, 297–323.
Zhao, W.J., Nelson, K.D., Project INDEPTH Team, 1993. Deep seismic reflection evidence for continental underthrusting beneath southern Tibet. Nature 366, 557–559.
Zhou, M., Malpas, J., Song, X., Robinson, P.T., Sun, M., Kennedy, A.K., Lesher, C.M., Keays, R.R., 2002. A temporal link between the Emeishan large igneous province (SW China) and the end-Guadalupian mass extinction. Earth and Planetary Science Letters 196, 113–122.
Zhu, B.Q., Mao, C.X., Lugmair, G.M., Macdougall, J.D., 1983. Isotopic and geochemical evidence for the origin of Plio–Pleistocene volcanic rocks near the Indo–Eurasian collisional margin at Tengchong, China. Earth and Planetary Science Letters 65, 263–275.